

Influence of numerical diffusion in high temperature flow ¹

M. Fey and R. Jeltsch

Research Report No. 91-10
Dezember 1991

Seminar für Angewandte Mathematik
Eidgenössische Technische Hochschule
CH-8092 Zürich
Switzerland

¹to appear in the Proceedings of the 9th GAMM Conference on Numerical Methods in Fluid Mechanics, 25–27. Sept. 1991, Lausanne, Vieweg-Verlag

Influence of numerical diffusion in high temperature flow

M. Fey and R. Jeltsch
Seminar für Angewandte Mathematik
Eidgenössische Technische Hochschule
CH-8092 Zürich
Switzerland

Research Report No. 91-10

Dezember 1991

Abstract

In high temperature flow it is necessary to introduce new physical phenomena to the governing equations. Chemical reactions and vibrational excitation of the molecules lead to inhomogeneous Euler equations with a source term and an additional equation of conservation of mass for each species. From the mathematical point of view we only get additional contact discontinuities for the different species. From the numerical perspective the treatment of the fluxes of partial densities has a large influence on the results. For a given shock-capturing scheme we discuss three methods to compute the fluxes of partial densities for the same total density flux. We compare the numerical diffusion for the different fluxes. In a two-dimensional testcase we illustrate the advantages and disadvantages of these schemes. The third one shows a good resolution of the strong gradients in the mass fractions for this special testcase.

Keywords: chemical reacting flow, numerical diffusion, stagnation point

Subject Classification: 65M05, 65G99

To appear in the Proceedings of the 9th GAMM Conference on Numerical Methods in Fluid Mechanics, 25–27. Sept. 1991, Lausanne, Vieweg-Verlag

1 Introduction

For a class of flow problems such as the reentry of a space vehicle or the conditions in a shock tube the numerical simulation becomes important. From the need to calculate the flow field around a double ellipse at an altitude of 70 km during the reentry, several different experiments were made concerning the numerical diffusion of the scheme. A more or less academic problem is the stagnation point temperature for an inviscid flow. This is a very sensitive value in the flow field which depends strongly on the composition of the gas. Due to the strong density and temperature gradients near the stagnation point, numerical diffusion becomes important. For small-scaled bodies these gradients are infinite so that most of the numerical schemes do not calculate the correct temperature as it was shown in [1]. This problem is an interesting example to examine the influence of numerical diffusion. We will explain our investigations for this testcase. First we present two ways to introduce chemical reactions into a standard Euler-solver. The first one is a straightforward procedure with a large amount of numerical diffusion. The second one based on the physical background of contact surfaces does not show the correct behavior in the steady state solution. The combination of both ideas then leads to an improved scheme with reduced numerical diffusion.

2 The governing equations

The equations describing the one-dimensional inviscid flow with chemical reactions are the Euler equations in the form

$$U_t + F(U)_x = S(U) \quad (1)$$

where

$$U = \begin{pmatrix} \varrho_1 \\ \vdots \\ \varrho_N \\ m \\ E \end{pmatrix}, \quad F(U) = \begin{pmatrix} \varrho_1 u \\ \vdots \\ \varrho_N u \\ mu + p \\ u(E + p) \end{pmatrix}, \quad S(U) = \begin{pmatrix} s_1(\varrho_1, \dots, \varrho_N, T) \\ \vdots \\ s_N(\varrho_1, \dots, \varrho_N, T) \\ 0 \\ 0 \end{pmatrix}. \quad (2)$$

Here ϱ_i , $i = 1, \dots, N$ denote the partial densities, m is the momentum and E the total energy including the formation enthalpy of the different species, p is the pressure, u the velocity and T the temperature of the gas. In the case

of chemical non-equilibrium the eigenvalues of the Jacobian matrix of $F(U)$ are $u - c, u, \dots, u, u + c$. c is the frozen speed of sound given by $c^2 = \gamma p / \varrho$ where ϱ is the total density and γ is the ratio of the heat capacities for constant pressure and constant volume. In comparison to a pure gas there are additional contact discontinuities due to the different species all moving with velocity u . Equation (1) is equivalent to

$$\hat{U}_t + F(\hat{U})_x = \hat{S}(\hat{U}) \quad (3)$$

with

$$\hat{U} = \begin{pmatrix} \varrho_1 \\ \vdots \\ \varrho_N \\ m \\ \hat{E} \end{pmatrix}, \quad \hat{S}(\hat{U}) = \begin{pmatrix} s_1(\varrho_1, \dots, \varrho_N, T) \\ \vdots \\ s_N(\varrho_1, \dots, \varrho_N, T) \\ 0 \\ -\sum_{i=1}^N h_i^0 s_i \end{pmatrix}. \quad (4)$$

\hat{E} is the total energy without the heat of formation, i.e.

$$E = \sum_{j=1}^N \varrho_j (e_j(T) + h_j^0) + \varrho \frac{u^2}{2} = \hat{E} + \sum_{j=1}^N \varrho_j h_j^0 \quad (5)$$

where $e_j(T)$ is the internal energy per unit mass of species j and h_j^0 the formation enthalpy.

3 The numerical scheme

The main underlying scheme is a finite volume method with the Van Leer flux vector splitting [3] to evaluate the fluxes at the cell interfaces. Starting from a discrete function U_i^n at time $n\Delta t$ at the point $i\Delta x$ we solve the inhomogeneous equations by an operator splitting approach. We first integrate the ordinary differential equation

$$\frac{\partial U}{\partial t} = S(U) \quad (6)$$

for an intermediate value $U_i^{n+1/2}$. In this step we use formulation (1) to avoid the source term in the energy equation. In the next step we solve the homogeneous Euler equation. We adapt the standard solver to chemical

reacting flow by the following procedure. First we rewrite the energy flux $F^E(U)$ to separate the heat of formation:

$$\begin{aligned} F^E(U) = u(E + p) &= u(\hat{E} + p) + \sum_{j=1}^N \varrho_j u h_j^0 \\ &= F^E(\hat{U}) + \sum_{j=1}^N h_j^0 F^{\varrho_j}(\hat{U}). \end{aligned} \quad (7)$$

So we get the total energy flux as the standard energy flux plus the sum of the formation enthalpy of each species times their density flux $F^{\varrho_j}(\hat{U})$. Since there are no reactions in this step the mass fractions Y^j in each cell are constant. For this step we reduce the system to

$$W_t + \hat{F}(W)_x = 0$$

with

$$W = W(U) = \begin{pmatrix} \sum_{j=1}^N \varrho_j \\ m \\ E - \sum_{j=1}^N \varrho_j h_j^0 \end{pmatrix} = \begin{pmatrix} \varrho \\ m \\ \hat{E} \end{pmatrix}, \quad \hat{F}(W) = \begin{pmatrix} m \\ mu + p \\ u(\hat{E} + p) \end{pmatrix}$$

by summing over all partial densities and removing the heat of formation. We update the values of W with the Van Leer flux vector splitting method for real gas. We have

$$W_i^{n+1} = W_i^n - \frac{\Delta t}{\Delta x} (\hat{F}_{i+1/2} - \hat{F}_{i-1/2}) \quad (8)$$

with

$$\hat{F}_{i+1/2} = \hat{F}_{i+1/2}(W_i^n, W_{i+1}^n) = F^+(W_i^n) + F^-(W_{i+1}^n).$$

The fluxes are

$$F^+(W) = \begin{cases} \hat{F}(W) & \text{if } u > c \\ 0 & \text{if } -c \geq u \end{cases}, \quad F^-(W) = \begin{cases} 0 & \text{if } u > c \\ \hat{F}(W) & \text{if } -c \geq u \end{cases},$$

and if $|u| \leq c$ then

$$\begin{aligned} F^{\varrho^\pm}(W) &= \pm \frac{\varrho}{4c} (u \pm c)^2, \\ F^{m^\pm}(W) &= \frac{\varrho}{4\gamma c} (u \pm c)^2 (2c \pm (\gamma - 1)u), \\ F^{\hat{E}^\pm}(W) &= \pm \frac{\varrho}{4c} (u \pm c)^2 \left[\frac{(2c \pm (\gamma - 1)u)^2}{2(\gamma^2 - 1)} + \frac{c^2}{\gamma} \left(\frac{\bar{\gamma}}{\bar{\gamma} - 1} - \frac{\gamma}{\gamma - 1} \right) \right]. \end{aligned}$$

$\bar{\gamma}$ is an averaged value of $\gamma = \gamma(T)$ over a temperature region.

With these properties we can construct the fluxes of the partial densities in a straightforward manner by setting

$$F_{i+1/2}^{\ell j} = Y_i^j \hat{F}^{\ell+}(W_i^n) + Y_{i+1}^j \hat{F}^{\ell-}(W_{i+1}^n). \quad (9)$$

In the second approach we take a closer look at the physics of a contact surface. Different compositions of the gas are separated by a contact discontinuity and remain separated. From the direction of this wave we can derive the movement of the different mass fractions (Fig. 1).

The propagation of this wave depends directly on the sign of the total mass flux. If this flux is positive then the contact surface moves to the right and vice versa. With this idea we can construct a second flux for the partial densities setting

$$F_{i+1/2}^{\ell j} = \begin{cases} Y_i^j \hat{F}_{i+1/2}^{\ell} & \text{if } \hat{F}_{i+1/2}^{\ell} > 0 \\ Y_{i+1}^j \hat{F}_{i+1/2}^{\ell} & \text{if } \hat{F}_{i+1/2}^{\ell} \leq 0 \end{cases}. \quad (10)$$

With the fluxes of the partial densities in (9) or (10),

$$F_{i+1/2}^m = \hat{F}_{i+1/2}^m$$

for the momentum, and

$$F_{i+1/2}^E = \hat{F}_{i+1/2}^E + \sum_{j=1}^N h_j^0 F_{i+1/2}^{\ell j} \quad (11)$$

for the energy we update the quantities in U in the same manner as in (8) using the intermediate state $U_i^{n+1/2}$ as the initial value.

$$U_i^{n+1} = U_i^{n+1/2} - \frac{\Delta t}{\Delta x} (F_{i+1/2} - F_{i-1/2}). \quad (12)$$

Both fluxes with (9) and (10) are consistent in the sense that $F_{i+1/2}(U, U) = F(U)$.

We now compare these fluxes. To keep the notation as simple as possible we set:

$$\begin{aligned} F_i^{\pm} &:= \hat{F}^{\ell\pm}(W(U_i^{n+1/2})) \\ F_{i+1/2} &:= \hat{F}_{i+1/2}^{\ell} \\ G_{i+1/2}^j &:= F_{i+1/2}^{\ell j} && \text{from (9)} \\ H_{i+1/2}^j &:= F_{i+1/2}^{\ell j} && \text{from (10)} \end{aligned}$$

We look at the difference

$$\begin{aligned}
& (H_{i+1/2}^j - H_{i-1/2}^j) - (G_{i+1/2}^j - G_{i-1/2}^j) \\
= & \begin{cases} Y_i^j(F_i^+ + F_{i+1}^-) - Y_{i-1}^j(F_{i-1}^+ + F_i^-) & \text{if } F_{i+1/2} > 0, F_{i-1/2} > 0 \\ Y_i^j(F_i^+ + F_{i+1}^-) - Y_i^j(F_{i-1}^+ + F_i^-) & \text{if } F_{i+1/2} > 0, F_{i-1/2} \leq 0 \\ Y_{i+1}^j(F_i^+ + F_{i+1}^-) - Y_{i-1}^j(F_{i-1}^+ + F_i^-) & \text{if } F_{i+1/2} \leq 0, F_{i-1/2} > 0 \\ Y_{i+1}^j(F_i^+ + F_{i+1}^-) - Y_i^j(F_{i-1}^+ + F_i^-) & \text{if } F_{i+1/2} \leq 0, F_{i-1/2} \leq 0 \end{cases} \\
& - \left(Y_i^j F_i^+ + Y_{i+1}^j F_{i+1}^- - Y_{i-1}^j F_{i-1}^+ - Y_i^j F_i^- \right) \\
= & \begin{cases} (-F_{i+1}^-)(Y_{i+1}^j - Y_i^j) + (-F_i^-)(Y_{i-1}^j - Y_i^j) & \text{if } F_{i+1/2} > 0, F_{i-1/2} > 0 \\ (-F_{i+1}^-)(Y_{i+1}^j - Y_i^j) + F_i^+(Y_{i-1}^j - Y_i^j) & \text{if } F_{i+1/2} > 0, F_{i-1/2} \leq 0 \\ F_{i+1}^+(Y_{i+1}^j - Y_i^j) + (-F_i^-)(Y_{i-1}^j - Y_i^j) & \text{if } F_{i+1/2} \leq 0, F_{i-1/2} > 0 \\ F_{i+1}^+(Y_{i+1}^j - Y_i^j) + F_i^+(Y_{i-1}^j - Y_i^j) & \text{if } F_{i+1/2} \leq 0, F_{i-1/2} \leq 0 \end{cases}
\end{aligned}$$

For subsonic flow, i.e. $|u| < c$, there exists a constant $K \in \mathbb{R}$ such that

$$\begin{aligned}
F^+ & \geq K > 0 \quad \text{and} \\
-F^- & \geq K > 0.
\end{aligned}$$

Then the fluxes in (9) and (10) can be compared yielding

$$G_{i+1/2}^j - G_{i-1/2}^j \approx H_{i+1/2}^j - H_{i-1/2}^j - K(Y_{i+1}^j - 2Y_i^j + Y_{i-1}^j)$$

and the additional numerical diffusion can be estimated by the last term. In this estimate only the fluxes in the partial densities are needed.

For the numerical tests we changed the geometry of the Antibes test-case from an ellipse to a cylinder. This does not change the values in the stagnation point, it only removes additional complications due to the non-symmetric mesh and the curved streamline ending at the stagnation point. For the cylinder we can calculate a solution by integrating an ODE system for the partial densities and the velocity along the streamline. Figures 2 – 4 show the solutions for different scalings of the body. The size of the body is proportional to the inverse of v_y , the derivative of the y-velocity component in the y-direction. We can see from the plots of density, temperature, and mass fraction of nitrogen atoms Y^N that the chemical reactions move more and more to the stagnation point when the body becomes smaller and smaller.

Test calculations with these two fluxes show an unacceptable property of the flux in (10). From the energy equation we get

$$\frac{\partial E}{\partial t} + \frac{\partial}{\partial x}(u(E + p)) = \frac{\partial E}{\partial t} + \frac{\partial}{\partial x}(u \varrho H) = 0. \quad (13)$$

In the steady state we have

$$0 = \frac{\partial}{\partial x}(u\rho H) = \rho u \frac{\partial}{\partial x} H + H \frac{\partial}{\partial x} \rho u. \quad (14)$$

Due to the conservation of mass the second term vanishes and thus H is constant along streamlines. Fig. 5 shows the total enthalpy H along the stagnation point streamline. For the flux in (10) the enthalpy increases drastically near the stagnation point in contrast to the standard Van Leer flux (9). This behavior can be explained by the following: The mass fractions Y^j are independent in different cells as they used to be due to the contact surface. The same holds for the heat of formation because in (11) the same flux of the partial densities is used. This contradicts equation (14) and the fact that the total enthalpy which includes the formation enthalpy is constant.

Therefore we define a third scheme. For the fluxes of the partial densities we keep the formula (10), but for the energy flux (11) we use the $F_{i+1/2}^{e_j}$ defined in (9):

$$F_{i+1/2}^{e_j} = \begin{cases} Y_i^j \hat{F}_{i+1/2}^{e^+} & \text{if } \hat{F}_{i+1/2}^{e^+} > 0 \\ Y_{i+1}^j \hat{F}_{i+1/2}^{e^-} & \text{if } \hat{F}_{i+1/2}^{e^-} \leq 0 \end{cases}$$

$$F_{i+1/2}^E = \hat{F}_{i+1/2}^E + \sum_{j=1}^N h_j^0 [Y_i^j \hat{F}^{e^+}(W_i^n) + Y_{i+1}^j \hat{F}^{e^-}(W_{i+1}^n)] \quad (15)$$

The resulting scheme is still consistent in the above sense. We now have a combination of both properties. The mass fractions are now nearly independent of the neighboring values and the numerical diffusion is reduced as shown above. On the other hand we introduce a mechanism to control the heat of formation over the cell interfaces in the energy flux.

The last sequence of figures shows the values of temperature, density, and mass fraction of nitrogen atoms for the three schemes with two different meshes. The size of the cell in front of the stagnation point is 0.5 mm and 0.2 mm, respectively.

4 Conclusions and Remarks

In the case of chemical reacting flow it is necessary to reduce the numerical diffusion. A comparison of the results seems to show that the combined scheme (15) gives a better approximation of the mass fractions than the standard Van Leer scheme (9). The investigations in this article are not

restricted to Van Leer's scheme, for some other methods like TVD or ENO it is also possible to replace the standard flux of partial densities by the one in (10).

From useful discussions with colleagues it seems that for some special Godunov schemes an increase of the total enthalpy in the steady state solution also results from the contact surface of the tangential velocity in a two dimensional flow. This contact surface has the same properties as those mentioned above.

References

- [1] Proceedings of the Antibes Workshop Part I (1990), to appear
- [2] K.E. Brenan, S.L. Campbell, L.R. Petzold, *Numerical Solution of Initial-Value Problems in Differential-Algebraic Equations*, North-Holland, New York, Amsterdam, London (1989)
- [3] B. VAN LEER, *Flux-Vector Splitting for the Euler Equations*, Lect. Notes in Phys. 170 (1982), pp 507-512

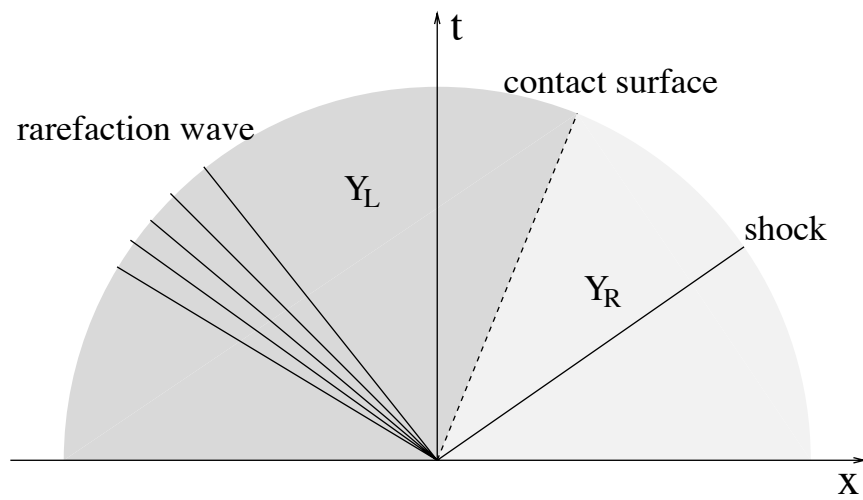


Figure 1: Separation of different mass fractions by the contact surface

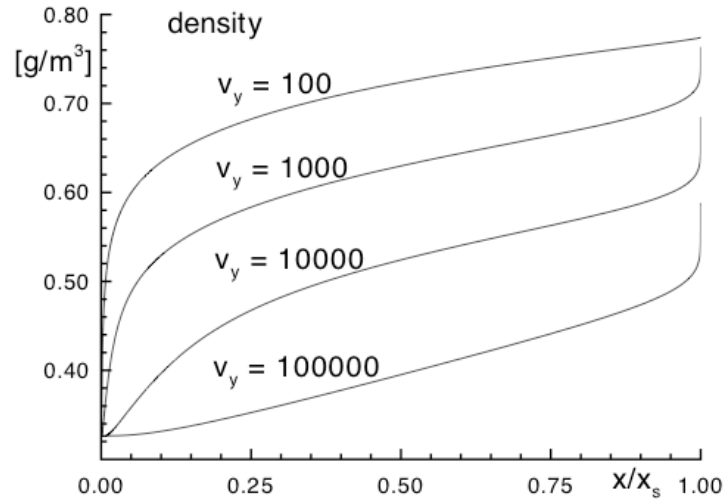


Figure 2: Density along the streamline with the ODE Solver DDASSL [2]

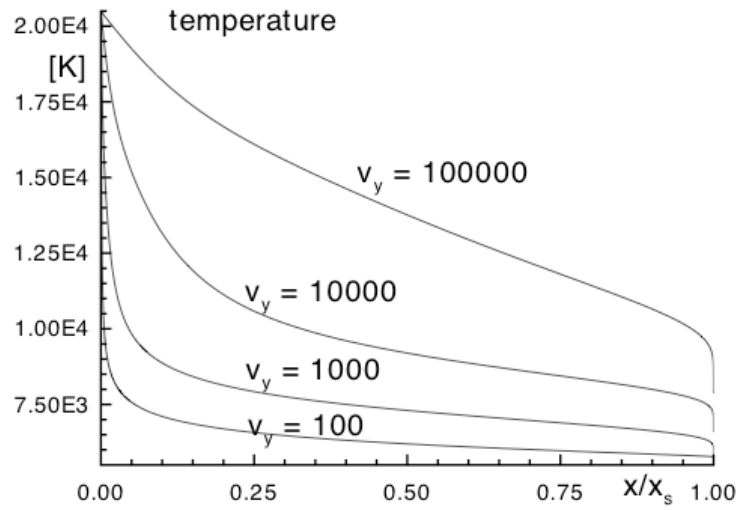


Figure 3: Temperature along the streamline with the ODE Solver DDASSL

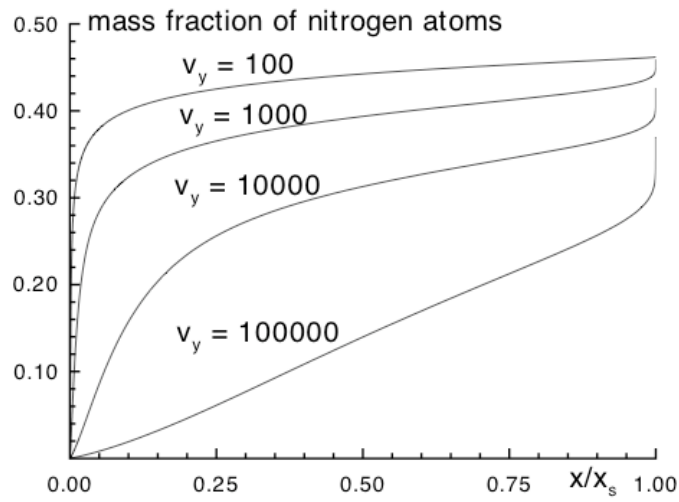


Figure 4: Mass fraction of nitrogen atoms along the streamline with the ODE Solver DDASSL

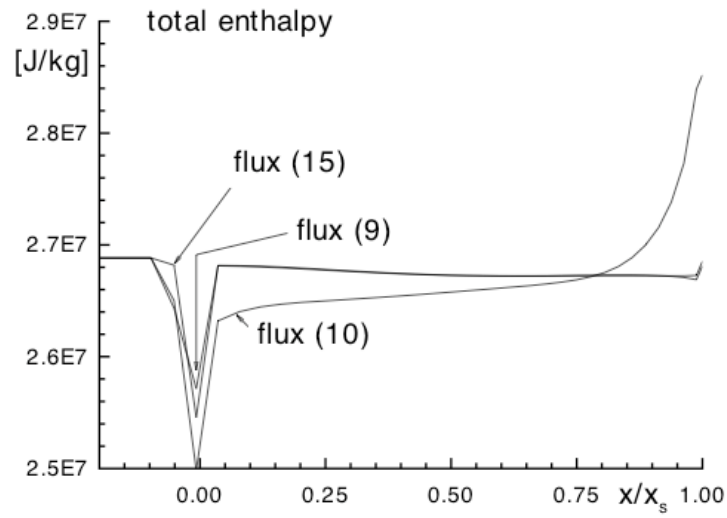


Figure 5: Total enthalpy along the streamline with different fluxes of partial densities

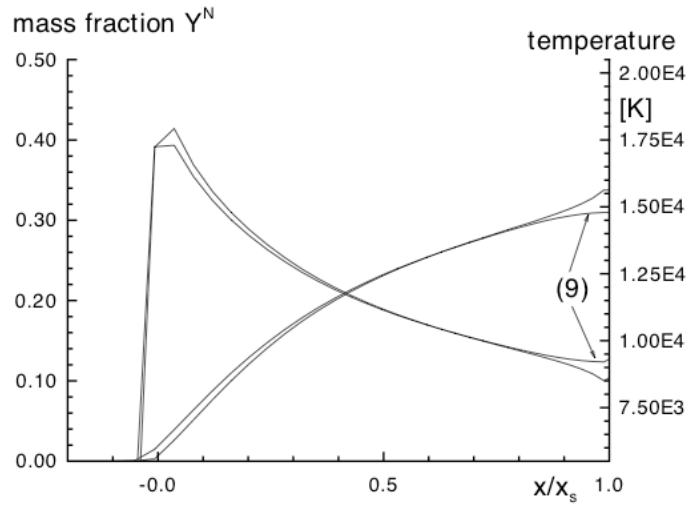


Figure 6: Solution with 0.5 mm cell size and fluxes (9) and (15).

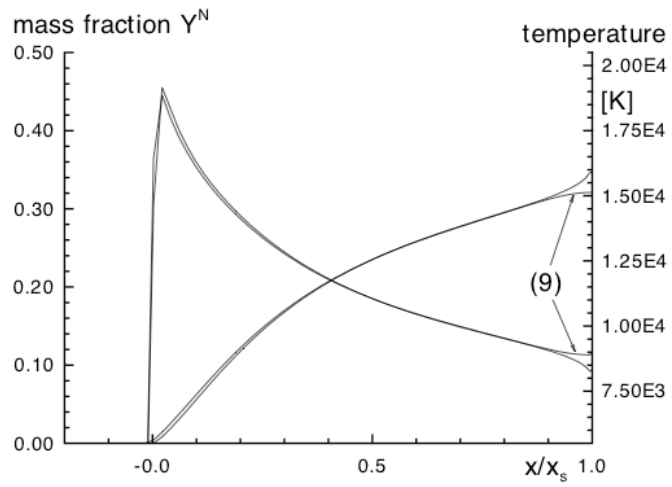


Figure 7: Solution with 0.2 mm cell size and fluxes (9) and (15).

Research Reports

Report No.	Authors	Title
91-10	M. Fey, R. Jeltsch	Influence of numerical diffusion in high temperature flow
91-09	R. J. LeVeque, R. Walder	Grid Alignment Effects and Rotated Methods for Computing Complex Flows in Astrophysics
91-08	Ch. Lubich, R. Schneider	Time discretization of parabolic boundary integral equations
91-07	M. Pirovino	On the Definition of Nonlinear Stability for Numerical Methods
91-06	Ch. Lubich, A. Ostermann	Runge-Kutta Methods for Parabolic Equations and Convolution Quadrature
91-05	C. W. Schulz-Rinne	Classification of the Riemann Problem for Two-Dimensional Gas Dynamics
91-04	R. Jeltsch, J. H. Smit	Accuracy Barriers of Three Time Level Difference Schemes for Hyperbolic Equations
91-03	I. Vecchi	Concentration-cancellation and Hardy spaces
91-02	R. Jeltsch, B. Pohl	Waveform Relaxation with Overlapping Splittings
91-01	R. Brawer, M. Pirovino	Das Bernoullische Potenzsummen-Problem und die Stirling-Zahlen 2. Art